Science behind the hunt for Flight 370 *pp. 947 & 963*

Incentives for antibiotic innovation *p. 967*

Toward atomic magnetic memory *pp. 976 & 988*

Science

$10
30 MAY 2014
sciencemag.org

AAAS

Inner life of the synapse

3D model yields realistic view of teeming proteins and organelles *p. 1023*

Composition of isolated synaptic boutons reveals the amounts of vesicle trafficking proteins

Benjamin G. Wilhelm *et al.*

Science **344**, 1023 (2014);
DOI: 10.1126/science.1252884

Here, we have disclosed that Sema3A and Sema7A function as retrograde signaling molecules that regulate developmental synapse elimination in the cerebellum. Our results suggest that Sema3A and Sema7A have opposite effects and are involved in different stages of synapse elimination (fig. S22). Because semaphorins and their receptors are expressed widely in the brain, it is highly likely that semaphorins play important roles in developmental synapse elimination in various brain areas.

REFERENCES AND NOTES

1. M. Kano, K. Hashimoto, *Curr. Opin. Neurobiol.* **19**, 154–161 (2009).
2. M. Watanabe, M. Kano, *Eur. J. Neurosci.* **34**, 1697–1710 (2011).
3. J. W. Lichtman, H. Colman, *Neuron* **25**, 269–278 (2000).
4. M. Kano *et al.*, *Cell* **83**, 1223–1231 (1995).
5. M. Kano *et al.*, *Neuron* **18**, 71–79 (1997).
6. F. Crepel, *Trends Neurosci.* **5**, 266–269 (1982).
7. N. Uesaka *et al.*, *J. Neurosci.* **32**, 11657–11670 (2012).
8. T. Mikuni *et al.*, *Neuron* **78**, 1024–1035 (2013).
9. K. Hashimoto *et al.*, *Proc. Natl. Acad. Sci. U.S.A.* **108**, 9987–9992 (2011).
10. K. Hashimoto, R. Ichikawa, K. Kitamura, M. Watanabe, M. Kano, *Neuron* **63**, 106–118 (2009).
11. F. Crepel, N. Delhaye-Bouchaud, J. L. Dupont, *Brain Res. Dev. Brain Res.* **1**, 59–71 (1981).
12. K. Hashimoto, M. Kano, *Neuron* **38**, 785–796 (2003).
13. S. Kakizawa, M. Yamasaki, M. Watanabe, M. Kano, *J. Neurosci.* **20**, 4954–4961 (2000).
14. K. Hashimoto *et al.*, *J. Neurosci.* **21**, 9701–9712 (2001).
15. T. Miyazaki, K. Hashimoto, H. S. Shin, M. Kano, M. Watanabe, *J. Neurosci.* **24**, 1734–1743 (2004).
16. R. J. Pasterkamp, *Nat. Rev. Neurosci.* **13**, 605–618 (2012).
17. R. J. Pasterkamp, J. J. Peschon, M. K. Spriggs, A. L. Kolodkin, *Nature* **424**, 398–405 (2003).
18. G. A. Scott, L. A. McClelland, A. F. Fricke, A. Fender, *J. Invest. Dermatol.* **129**, 954–963 (2009).
19. H. Hirai, T. Torashima, Japanese Patent 4975733 (2012).

ACKNOWLEDGMENTS

We thank A. Nienhuis for the gifts of the lentiviral backbone vector and the packaging plasmid. A Purkinje cell–tropic viral vector has been patented (*19*). We also thank K. Kitamura, K. Hashimoto, Y. Sugaya, and M. Mahoney for helpful discussions and K. Matsuyama, M. Sekiguchi, M. Watanabe, S. Tanaka, and A. Koseki for technical assistance. This work was supported by Grants-in-Aid for Scientific Research (21220006 and 25000015 to M.K., 19100005 and 24220007 to M.W., and 23650160 to N.U.), the Funding Program for Next Generation World-Leading Researchers (LS021) to H.H., the Strategic Research Program for Brain Sciences (Development of Biomarker Candidates for Social Behavior), Comprehensive Brain Science Network, and the Global Center of Excellence Program (Integrative Life Science Based on the Study of Biosignaling Mechanisms) from the Ministry of Education, Culture, Sports, Science and Technology of Japan. H.H. and T. Torashima are inventors on a Japanese and a U.S. patent application for a Purkinje cell–tropic viral vector (the modified L7 promoter sequences that enable robust transgene expression specifically in cerebellar Purkinje cells, PCT/JP2007/055017 filed on 7 March 2007 and US20100146649), which is owned by Japan Science and Technology Agency (*19*). Materials described here are available from H.H. and A. Nienhuis, subject to a material transfer agreement (MTA) with Gunma University for the modified L7 promoter and an MTA with St. Jude Children's Research Hospital and the George Washington University for the pCL20c MSCV-GFP. Additional data can be found in the supplementary materials.

SUPPLEMENTARY MATERIALS

www.sciencemag.org/content/344/6187/1020/suppl/DC1
Materials and Methods
Figs. S1 to S22
Tables S1 to S3
References (*20*–*26*)

21 February 2014; accepted 6 May 2014
Published online 15 May 2014;
10.1126/science.1252514

SYNAPSES

Composition of isolated synaptic boutons reveals the amounts of vesicle trafficking proteins

Benjamin G. Wilhelm,[1,2] Sunit Mandad,[3]* Sven Truckenbrodt,[1,5]* Katharina Kröhnert,[1] Christina Schäfer,[1] Burkhard Rammner,[1] Seong Joo Koo,[6] Gala A. Claßen,[6] Michael Krauss,[6] Volker Haucke,[6] Henning Urlaub,[3,4] Silvio O. Rizzoli[1]†

Synaptic vesicle recycling has long served as a model for the general mechanisms of cellular trafficking. We used an integrative approach, combining quantitative immunoblotting and mass spectrometry to determine protein numbers; electron microscopy to measure organelle numbers, sizes, and positions; and super-resolution fluorescence microscopy to localize the proteins. Using these data, we generated a three-dimensional model of an "average" synapse, displaying 300,000 proteins in atomic detail. The copy numbers of proteins involved in the same step of synaptic vesicle recycling correlated closely. In contrast, copy numbers varied over more than three orders of magnitude between steps, from about 150 copies for the endosomal fusion proteins to more than 20,000 for the exocytotic ones.

The quantitative organization of cellular pathways is not well understood. One well-researched membrane trafficking pathway, synaptic vesicle recycling, occupies its own compartment, the synaptic bouton, and can therefore be studied in isolation. It is a relatively simple pathway, comprising only a few steps (*1*–*3*). First, neurotransmitter-filled synaptic vesicles dock to the release site (active zone), are primed for release, and then fuse with the plasma membrane (exocytosis). The vesicle molecules are later sorted and retrieved from the plasma membrane (endocytosis). An additional sorting step in an early endosome (*3*–*5*) may take place before the vesicle refills with neurotransmitter.

To quantify the organization of synaptic vesicle recycling, we first purified synaptic boutons (synaptosomes) from the cellular layers of the cortex and cerebellum of adult rats, using a modified version (*6*) of a classical brain fractionation protocol (*7*) (Fig. 1A). The different cellular components were separated by Ficoll density gradients, resulting in a heterogeneous sample, which we first analyzed by electron microscopy. About 58.5% of all organelles were resealed, vesicle-loaded synaptosomes (fig. S1). Most of the remaining organelles, such as mitochondria (~20%) and myelin (8%) (fig. S1), contained few proteins relevant to synaptic vesicle recycling and thus did not bias synaptic protein quantification. The electron microscopy analysis of the synaptosomes also provided their spatial parameters (size, surface, and volume), which are critical in understanding protein concentrations (Fig. 1, B and C).

Before proceeding to investigate the synaptic protein copy numbers, we tested whether the synaptosomes lost a significant proportion of their proteins during the purification procedure. We compared the amounts of 27 soluble proteins and 2 transmembrane proteins in synaptosomes and in undisturbed synapses from brain slices, using fluorescence microscopy (fig. S2, A and B). The large majority of the proteins exhibited no significant changes after synaptosome purification (fig. S2C).

Having verified that the purification procedure maintains the protein composition of the synaptic bouton, we used quantitative immunoblotting to determine the amount of protein of interest per microgram of synaptosomes for 62 synaptic proteins (Fig. 1, D and E). To transform this value into copy numbers per synaptosome, we determined the number of particles in the synaptosome preparation by fluorescence microscopy (~17 million) (fig. S3) and the fraction represented by synaptosomes by electron microscopy (fig. S1, A and B) and by immunostaining for synaptic markers (fig. S1B). Both measurements indicate that ~58% of all particles are synaptosomes, ~9.95 million synaptosomes per microgram.

The results we obtained for all proteins tested are included in table S1. Despite the heterogeneous preparation we started with, our results are very close to synaptic vesicles purified to more than 95% (*8*), taking into account the

[1]Department of Neuro- and Sensory Physiology, University of Göttingen Medical Center, European Neuroscience Institute, Cluster of Excellence Nanoscale Microscopy and Molecular Physiology of the Brain, Göttingen, Germany. [2]International Max Planck Research School Neurosciences, 37077 Göttingen, Germany. [3]Bioanalytical Mass Spectrometry Group, Max-Planck-Institute for Biophysical Chemistry, 37077 Göttingen, Germany. [4]Bioanalytics, Department of Clinical Chemistry, University Medical Center Göttingen, 37075 Göttingen, Germany. [5]International Max Planck Research School Molecular Biology, 37077 Göttingen, Germany. [6]Leibniz Institut für Molekulare Pharmakologie, Department of Molecular Pharmacology and Cell Biology, Robert-Rössle-Strasse 10, 13125 Berlin, Germany.
*These authors contributed equally to this work. **†Corresponding author. E-mail: srizzol@gwdg.de**

known fractions of these proteins on the synaptic plasma membrane (*9*, *10*) (Fig. 1F). We only detected a sizeable difference for synaptic vesicle 2 (SV2) [12 copies per synaptic vesicle in our study, versus 1.7 for (*8*)]. A more recent study, using an antibody-based approach that is likely to underestimate the copy numbers of abundant synaptic vesicle proteins, found about five SV2 molecules per vesicle (*11*).

The immunoblot analysis also provided the total mass of each protein per microgram of synaptosome preparation, which could be translated to percentage of the total protein in the preparation. Our quantification of synaptic proteins addressed ~23% of the total protein in the preparation. Because the synaptosomes make ~58% of the preparation, our quantification thus addressed ~40.5% of the total protein in synaptosomes (without presynaptic mitochondria). To test and extend these values, we turned to quantitative mass spectrometry, using a label-free approach, intensity-based absolute quantification (iBAQ) (*12*). iBAQ estimates the abundance of particular proteins by summing the intensities of all peptides derived from them and then normalizing to the total possible number of peptides. We compared the peptides derived from recombinant synaptic proteins (same as those used for quantitative immunoblotting) from human Universal Protein Standards (UPS2) and finally from synaptosomes, using a hybrid mass spectrometer. iBAQ values were then calculated using MaxQuant (*13*) and the Andromeda search engine (*14*), and the amounts of proteins present in synaptosomes were determined by linear regression. The estimates obtained by iBAQ correlated well with the immunoblotting results (fig. S4). The iBAQ approach generated abundance estimates for ~1100 additional proteins in the preparation (see table S2 for a number of well-known proteins relevant to synaptic activity; see table S3 for all other proteins). All quantified proteins (iBAQ and immunoblot analysis) added up to ~88.4% of the protein weight of the entire synaptosome preparation (obtained

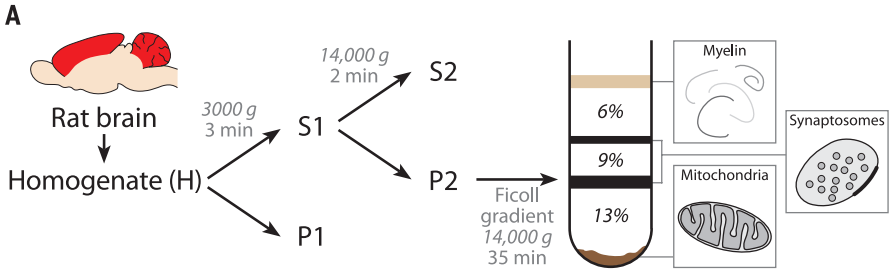

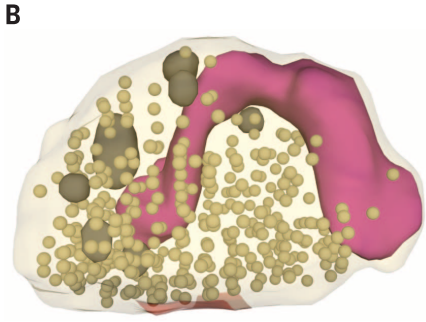

C

Physical characteristics of the average synaptosome	
Volume	0.37 ± 0.04 μm³
Surface	2.31 ± 0.14 μm²
Number of vesicles	383.7 ± 37.9
Volume of vesicles	0.015 ± 0.001 μm³
Inter-vesicle distance	59.15 ± 0.37 nm
Surface of active zone	0.070 ± 0.014 μm²
Volume of mitochondria	0.12 ± 0.02 μm³

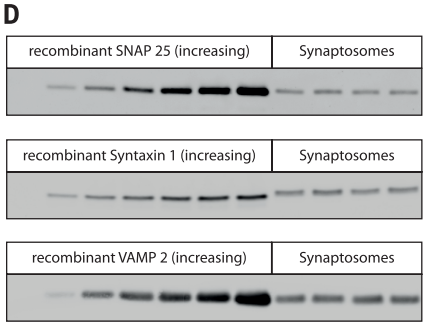

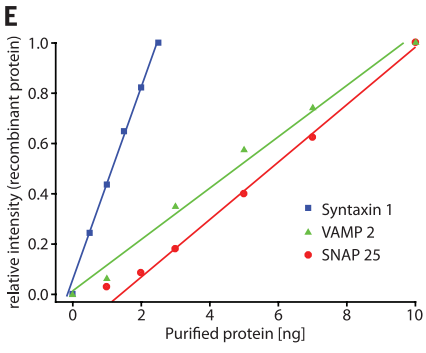

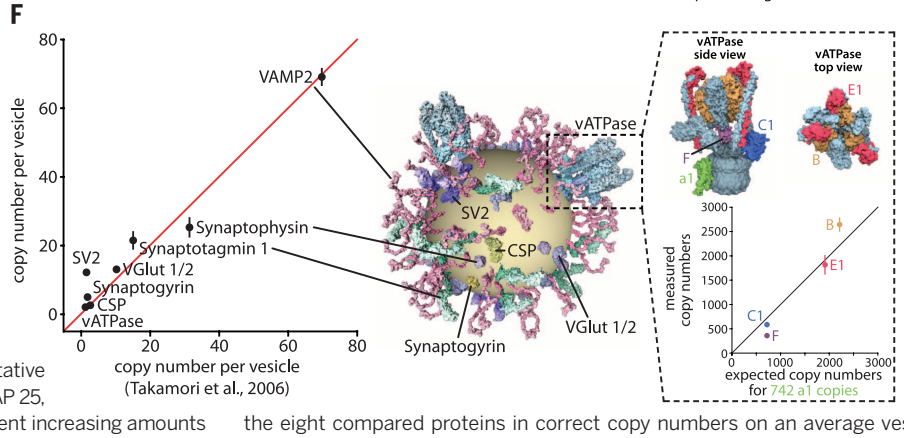

Fig. 1. Physical characteristics of the average synaptosome. (**A**) Schema illustrating the purification of synaptosomes. See the supplementary materials for details. (**B**) Serial electron micrographs of purified synaptosomes were used to reconstruct entire synapses. The plasma membrane is depicted in light beige, the active zone in red, synaptic vesicles in dark beige, larger organelles in dark gray, and mitochondria in purple. This synaptosome resembles the average physical parameters (C) and was used to model the average presynaptic terminal (Fig. 3). (**C**) Table listing the average physical parameters of synaptosomes. The values represent mean ± SEM of 65 reconstructions from four independent synaptosome preparations. (**D**) Quantitative immunoblots of the three synaptic SNARE proteins (SNAP 25, syntaxin 1, and VAMP 2). The lanes on the left represent increasing amounts of the purified protein of interest, forming a standard curve (protein amount versus band intensity). The different synaptosome samples are depicted in the four lanes on the right. (**E**) Standard curves of the three SNARE proteins obtained from the immunoblots depicted in (D). Linear regression was used to determine the absolute amount of the protein of interest in the synaptosomes. (**F**) (Left) The copy numbers for eight major synaptic vesicle proteins, normalized to the number of synaptic vesicles per synaptosome, are compared with the numbers obtained in a previous quantification of synaptic vesicles (*8*). The red line represents identity. (Middle) The model shows the eight compared proteins in correct copy numbers on an average vesicle. (Right) Correlation between the copy numbers of different vATPase subunits (highlighted in different colors in the vATPase model, above the graph). The immunoblot quantification of the a1 subunit (green; only the transmembrane part is shown) suggests the presence of 742 vATPase complexes per bouton. The copy numbers of the B, C, E, and F subunits (derived from iBAQ mass spectrometry) are plotted against their expected stoichiometries for 742 complexes. The stoichiometry of the different vATPase subunits was obtained from (*34*). The black line represents identity. All data represent means ± SEM from four independent preparations.

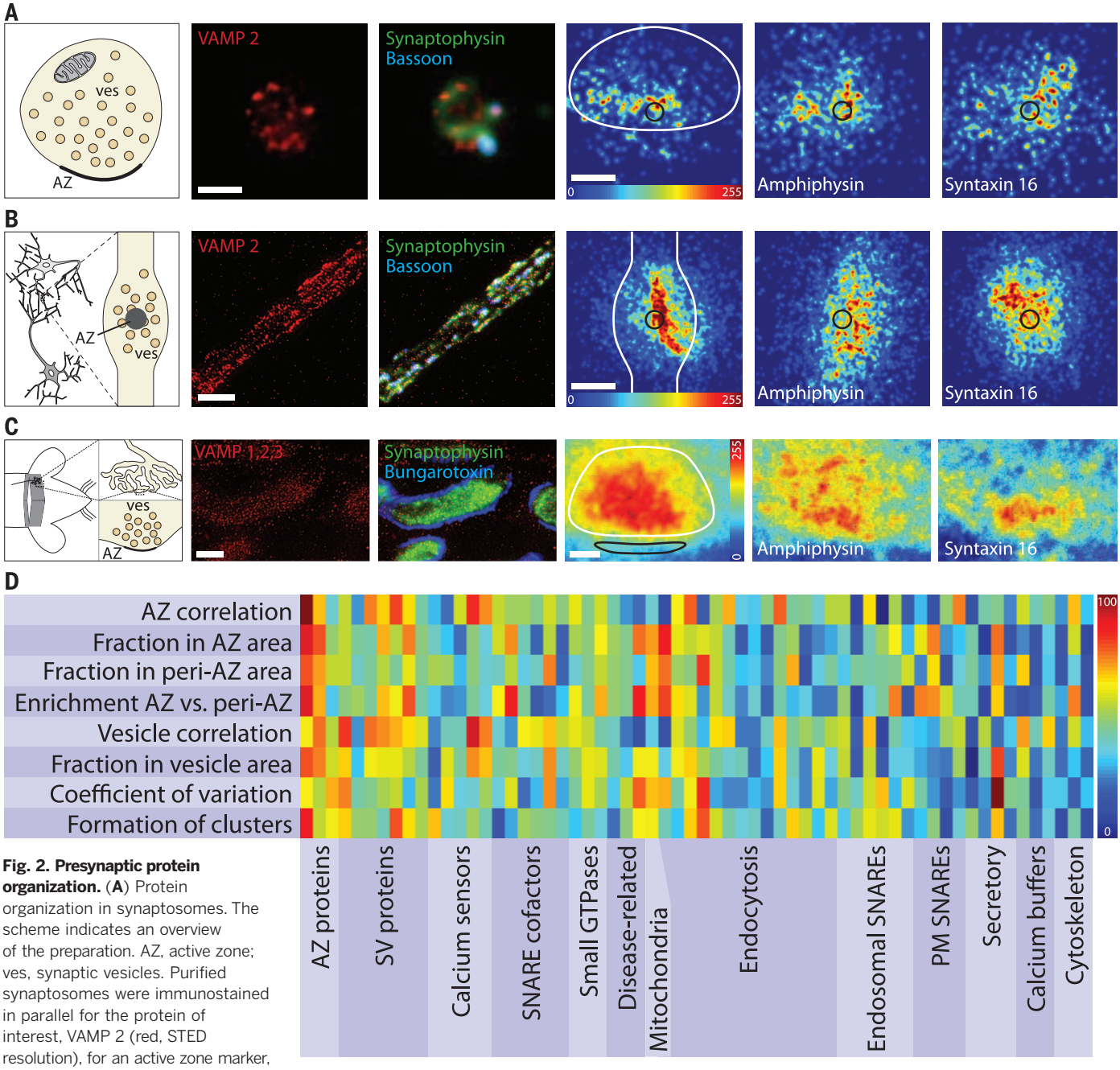

Fig. 2. Presynaptic protein organization. (**A**) Protein organization in synaptosomes. The scheme indicates an overview of the preparation. AZ, active zone; ves, synaptic vesicles. Purified synaptosomes were immunostained in parallel for the protein of interest, VAMP 2 (red, STED resolution), for an active zone marker, bassoon (blue, confocal resolution), and for a vesicle marker, synaptophysin (green, confocal resolution). The fourth panel shows the relative spatial distribution of VAMP 2 as obtained from average images (several hundred synapses from two independent experiments; see the supplementary materials for further details). The putative outline of the synapse is indicated by the white line, the active zone by the black circle; the relative spatial abundance is color-coded (see color bar). Scale bars are 500 nm (image panels) and 200 nm (fourth panel). The last two panels on the right are density distributions for two additional presynaptic proteins, amphiphysin and syntaxin 16. Scale bar is 200 nm. (**B**) Protein organization in hippocampal cultures. Details as in (A). Scale bars are 2 μm and 200 nm, respectively. (**C**) Protein organization in the mouse neuromuscular junction. Instead of immunostaining for bassoon, the active zone position was obtained by labeling postsynaptic acetylcholine receptors with bungarotoxin. All other details as in (A). Scale bars are 2 μm and 500 nm, respectively. Imaging data for all the other proteins are provided in fig. S6. (**D**) Different spatial parameters were measured for each of the 62 proteins we imaged, as indicated by the labeling of the rows. Parameter values were normalized to the maximum (100%). All values are indicated according to the color scale (right). The proteins are grouped according to functional categories: active zone proteins (bassoon, piccolo, and RIM1), synaptic vesicle proteins (synaptophysin, VGlut 1/2, VAMP 2, VAMP 1, SV2 A/B, synapsin I/II, and synaptogyrin 1), calcium sensor proteins (synaptotagmin 2, synaptotagmin 1, synaptotagmin 7, doc 2A/B, and calmodulin), SNARE cofactors (CSP, Munc13a, Munc18a, NSF, α-SNAP, and complexin 1/2), small guanosine triphosphatases (GTPases) (Rab3, Rab5, and Rab7), disease-related proteins (α/β-synuclein, APP, and β-secretase), mitochondrial proteins (VDAC), endocytosis proteins (AP-2 mu2, SGIP1, synaptojanin, epsin 1, clathrin heavy chain, clathrin light chain, dynamin 1,2,3, endophilin I,II,III, amphiphysin, Hsc70, intersectin 1, PIPK Iγ, AP 180, and syndapin 1), endosomal SNAREs (syntaxin 13, syntaxin 16, syntaxin 7, syntaxin 6, Vti1a, and VAMP4), plasma membrane SNAREs (syntaxin 1, SNAP 23, SNAP 25, and SNAP 29), general secretory proteins (CAPS, SCAMP 1, SGTα, and vATPase a1), calcium buffer proteins (calbindin, calretinin, and parvalbumin), and cytoskeletal proteins (actin, septin 5, and tubulin).

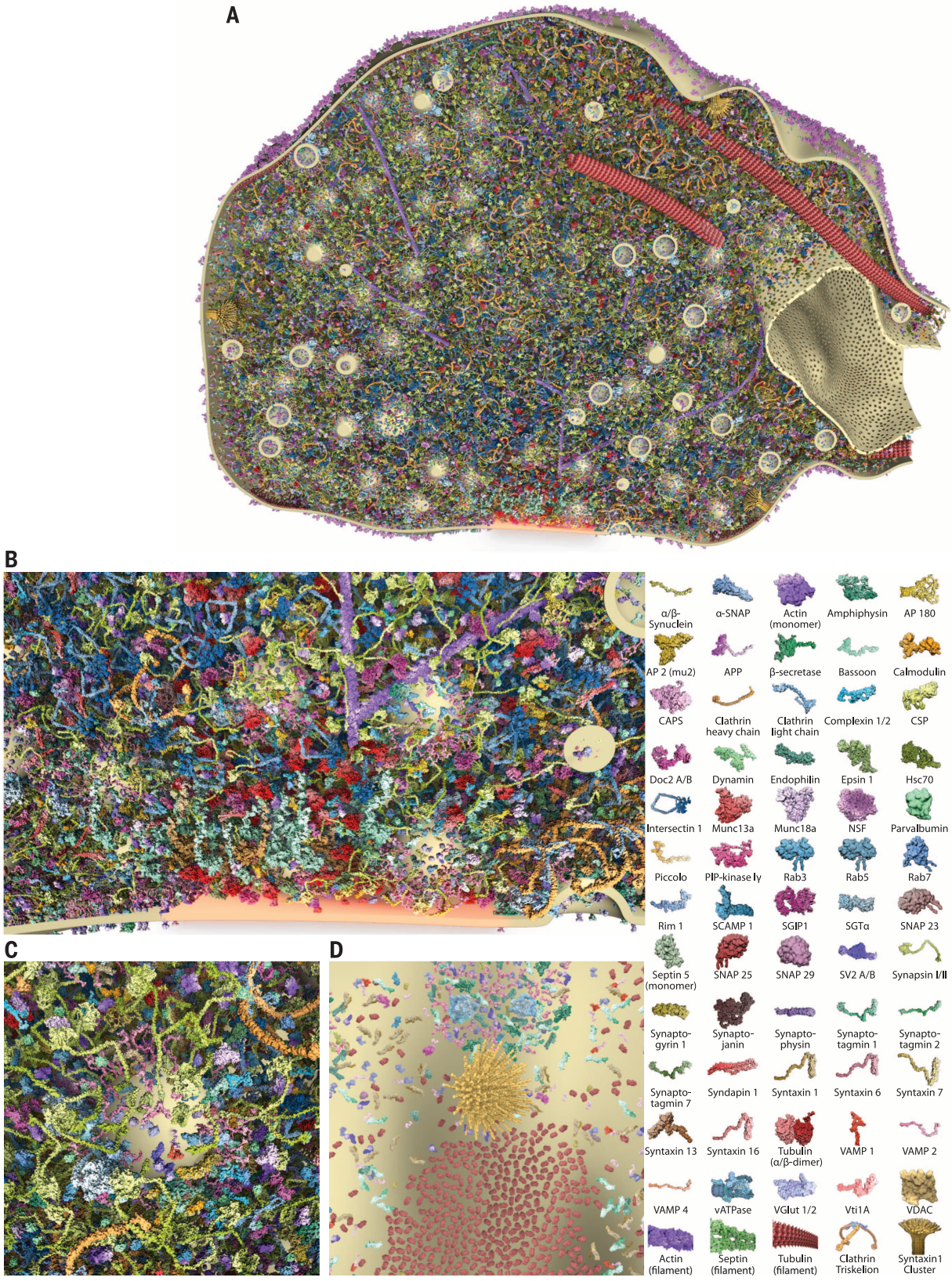

Fig. 3. A 3D model of synaptic architecture. (**A**) A section through the synaptic bouton, indicating 60 proteins. The proteins are shown in the copy numbers indicated in tables S1 and S2 and in positions determined according to the imaging data (Fig. 2 and fig. S6) and to the literature (see fig. S6 for details). (**B**) High-zoom view of the active zone area. (**C**) High-zoom view of one vesicle within the vesicle cluster. (**D**) High-zoom view of a section of the plasma membrane in the vicinity of the active zone. Clusters of syntaxin (yellow) and SNAP 25 (red) are visible, as well as a recently fused synaptic vesicle (top). The graphical legend indicates the different proteins (right). Displayed synaptic vesicles have a diameter of 42 nm.

by summing the percentages indicated in tables S1 to S3).

The members of heteromultimeric complexes, such as the vesicular adenosine triphosphatase (vATPase), were present in the correct (expected) stoichiometries (Fig. 1F), verifying the accuracy of our quantification procedure. The copy numbers of proteins known to be involved in a particular step of synaptic vesicle recycling correlated remarkably well. This observation applied to the exocytotic fusion proteins [SNAREs (fig. S5B), whose abundance was only matched by actin and tubulin (fig. S5M)], to proteins involved in fusion regulation [SNARE-binding or priming proteins (fig. S5C)], to proteins of the clathrin-mediated endocytosis pathway (fig. S5E), to endosomal or constitutive fusion proteins (fig. S5D), to structural vesicle cluster proteins (fig. S5F), to active zone proteins (fig. S5G), to major synaptic vesicle constituents (fig. S5H), or to adhesion proteins (fig. S5I). Proteins involved in membrane trafficking pathways unrelated to synaptic vesicle recycling, such as the exocyst pathway (fig. S5J), were not abundant. There was no correlation between structurally similar proteins, such as those of the Rab or septin families (fig. S5, K and L). Protein copy numbers are high in some steps of the vesicle recycling pathway but much lower in other steps. For example, the exocytotic SNAREs were present in 20,100 to 26,000 copies, despite the fact that one vesicle fusion event requires the formation of only one to three SNARE complexes, which contain one copy of each of the three SNAREs (*15*–*17*). SNARE-interacting proteins were found at copy numbers of one to several thousands (Munc13a, Munc18a, complexin I, and complexin II) (fig. S5C). In contrast, only ~4000 clathrin molecules and 2300 dynamin molecules were present in the average synapse. Because at least 150 to 180 copies of clathrin are needed for one recycling vesicle (*18*, *19*), the entire clathrin complement of the synapse would be sufficient for the simultaneous endocytosis of only 7% of all vesicles. The dynamin complement of the synapse was only sufficient for 11% of the vesicles, taking into account that at least 52 copies, corresponding to two adjacent dynamin rings, are needed for one pinch-off event (*20*). Finally, the endosomal SNAREs, which form tetrameric complexes containing one copy of each SNARE (*4*, *6*), were even less abundant (50 to 150 copies) than the endocytotic cofactors.

For some proteins, a strong enrichment in the location where they function may compensate for their low copy numbers. Conversely, abundant proteins may be scattered throughout the synaptic space, which would render their concentrations fairly low at individual sites. To estimate the influence of protein localization, we selected 62 proteins and analyzed them by immunostaining and fluorescence microscopy. We used stimulated emission depletion (STED) (*21*), a diffraction-unlimited technique, to investigate protein positions with a resolution of ~40 nm (Fig. 2A). To avoid bias owing to possible artifacts connected to the brain homogenization procedure required for generating synaptosomes, we also studied two additional preparations: cultured hippocampal neurons (Fig. 2B) and the levator auris longus neuromuscular junction (Fig. 2C), acutely dissected from adult animals (*22*).

We analyzed the proteins of interest in relation to the positions of the release site (identified by marking active zone proteins) and of the vesicle cluster (visualized by staining for the protein that is most strongly enriched in purified synaptic vesicles, synaptophysin) (*8*). We averaged single synapses by overlapping their active zones and rotating the images until reaching the best possible alignment of the vesicle cluster and of the protein of interest. This procedure provided an overview of the relative spatial distribution of each protein. Overall, many of the protein distributions were similar (Fig. 2, A to C, and fig. S6). Active zone proteins were mostly confined to the active zone areas. Most of the other proteins could be found throughout the synaptic boutons [albeit they were enriched to different levels in areas such as the active zone or the vesicle cluster (Fig. 2D); see fig. S7, A to H, for a more detailed analysis of differences between the proteins]. These observations are consistent with the presence of most of the proteins on purified synaptic vesicles (*8*) and with the fact that the synaptic vesicle cluster occupies much of the synaptic bouton volume (Fig. 1B). Thus, for the majority of proteins, localization does not appear to compensate for low copy numbers.

Although the imaging parameters measured above did not pinpoint actual positions within the synapse, they allowed us to make broad estimates for the organization of each protein (fig. S7I). We used the data to generate a three-dimensional (3D) model containing 60 proteins placed within a typical synaptic volume (obtained from an individual electron microscopy reconstruction whose parameters were close to synaptosome averages) (Fig. 3). The proteins were modeled in atomic detail, according to their known molecular structures, and were placed in the synaptic space according to the information provided by the STED images and the literature (Fig. 2 and fig. S6). For example, the SNARE molecules syntaxin 1 and SNAP 25 are shown in clusters with a specific organization (*23*–*25*). The hippocampal culture images (Fig. 2B) were used to obtain an additional set of data, the correlation of protein amounts with synapse size [judged from the amount of vesicles (*26*) (fig. S6)]. The copy numbers of some proteins increase linearly with synapse size; others, including most endocytotic proteins, follow an exponential curve, which implies that small synapses contain proportionally larger amounts of these proteins than large synapses.

We used the modeled volumes of the proteins to calculate the fraction of the synaptic volume that they occupy. This value, ~7% of the synaptosome volume (excluding mitochondria), is comparable to the space occupied by the synaptic vesicles (~6%, derived from the electron microscopy measurements). These low values could lead to the impression that the synaptic volume is not densely populated by proteinaceous structures. However, the 3D model suggests that the synaptic space is rather crowded, especially inside the vesicle cluster and at the active zone (Fig. 3, A to C, and movie S1). This probably places constraints on both organelle and protein diffusion. The high copy numbers of exocytosis-related proteins may have evolved as a mechanism to cope with these constraints, to ensure the high speed of neurotransmitter release. In contrast, endocytosis can take place for many tens of seconds after exocytosis. This allows endocytosis to proceed with proportionally lower numbers of cofactor proteins. In principle, the synaptic boutons could increase the speed of endocytosis by accumulating larger amounts of endocytotic proteins. This, however, would result in an even greater congestion of the synaptic space, which presumably might perturb synaptic function. A simpler solution for the problem of balancing rapid release with slow vesicle retrieval appears to have been to maintain a large enough reservoir of vesicles (*22*, *27*, *28*).

Our data reveal a correlation between the copy numbers of proteins involved in the same steps of synaptic vesicle recycling. The mechanisms behind this correlation are unclear. A simple hypothesis would be that such proteins either are produced together or are transported to the synapse together. However, these proteins have different lifetimes (*29*) and are transported from the neuronal cell body on different precursors (*30*). One possible explanation, at least for the soluble cofactor proteins, is that the synaptic vesicle cluster regulates their number. The vesicles are known to bind to and buffer such proteins (*22*, *31*–*33*), thereby retaining in the synapse only a defined number of cofactors. Such mechanisms do not apply, however, to transmembrane proteins, whose regulation remains to be determined.

REFERENCES AND NOTES

1. V. Haucke, E. Neher, S. J. Sigrist, *Nat. Rev. Neurosci.* **12**, 127–138 (2011).
2. R. Jahn, D. Fasshauer, *Nature* **490**, 201–207 (2012).
3. T. C. Südhof, *Annu. Rev. Neurosci.* **27**, 509–547 (2004).
4. P. Hoopmann *et al.*, *Proc. Natl. Acad. Sci. U.S.A.* **107**, 19055–19060 (2010).
5. V. Uytterhoeven, S. Kuenen, J. Kasprowicz, K. Miskiewicz, P. Verstreken, *Cell* **145**, 117–132 (2011).
6. S. O. Rizzoli *et al.*, *Traffic* **7**, 1163–1176 (2006).
7. D. G. Nicholls, T. S. Sihra, *Nature* **321**, 772–773 (1986).
8. S. Takamori *et al.*, *Cell* **127**, 831–846 (2006).
9. F. Opazo *et al.*, *Traffic* **11**, 800–812 (2010).
10. M. Darna *et al.*, *J. Biol. Chem.* **284**, 4300–4307 (2009).
11. S. A. Mutch *et al.*, *J. Neurosci.* **31**, 1461–1470 (2011).
12. B. Schwanhäusser *et al.*, *Nature* **473**, 337–342 (2011).
13. J. Cox, M. Mann, *Nat. Biotechnol.* **26**, 1367–1372 (2008).
14. J. Cox *et al.*, *J. Proteome Res.* **10**, 1794–1805 (2011).
15. R. Mohrmann, H. de Wit, M. Verhage, E. Neher, J. B. Sørensen, *Science* **330**, 502–505 (2010).
16. R. Sinha, S. Ahmed, R. Jahn, J. Klingauf, *Proc. Natl. Acad. Sci. U.S.A.* **108**, 14318–14323 (2011).
17. G. van den Bogaart *et al.*, *Nat. Struct. Mol. Biol.* **17**, 358–364 (2010).

18. Y. Cheng, W. Boll, T. Kirchhausen, S. C. Harrison, T. Walz, *J. Mol. Biol.* **365**, 892–899 (2007).
19. H. T. McMahon, E. Boucrot, *Nat. Rev. Mol. Cell Biol.* **12**, 517–533 (2011).
20. A. V. Shnyrova *et al.*, *Science* **339**, 1433–1436 (2013).
21. K. I. Willig, S. O. Rizzoli, V. Westphal, R. Jahn, S. W. Hell, *Nature* **440**, 935–939 (2006).
22. A. Denker *et al.*, *Proc. Natl. Acad. Sci. U.S.A.* **108**, 17177–17182 (2011).
23. D. Bar-On *et al.*, *J. Biol. Chem.* **287**, 27158–27167 (2012).
24. J. J. Sieber, K. I. Willig, R. Heintzmann, S. W. Hell, T. Lang, *Biophys. J.* **90**, 2843–2851 (2006).
25. J. J. Sieber *et al.*, *Science* **317**, 1072–1076 (2007).
26. V. N. Murthy, T. Schikorski, C. F. Stevens, Y. Zhu, *Neuron* **32**, 673–682 (2001).
27. V. Marra *et al.*, *Neuron* **76**, 579–589 (2012).
28. T. Rose, P. Schoenenberger, K. Jezek, T. G. Oertner, *Neuron* **77**, 1109–1121 (2013).
29. L. D. Cohen *et al.*, *PLOS ONE* **8**, e63191 (2013).
30. D. Bonanomi, F. Benfenati, F. Valtorta, *Prog. Neurobiol.* **80**, 177–217 (2006).
31. A. Denker, K. Kröhnert, J. Bückers, E. Neher, S. O. Rizzoli, *Proc. Natl. Acad. Sci. U.S.A.* **108**, 17183–17188 (2011).
32. O. Shupliakov, *Neuroscience* **158**, 204–210 (2009).
33. S. O. Rizzoli, *EMBO J.* **33**, 788–822 (2014).
34. N. Kitagawa, H. Mazon, A. J. R. Heck, S. Wilkens, *J. Biol. Chem.* **283**, 3329–3337 (2008).

ACKNOWLEDGMENTS

We thank the following collaborators for providing purified proteins and antibodies: R. Jahn, C. Griesinger, B. Shwaller, and A. Roux. We thank H. Martens for technical help and support, B. Rizzoli for helpful comments on the manuscript, and T. Sargeant for providing the carve source code for creation of the voltage-dependent anion channel (VDAC)-based mitochondrial membrane cut-outs. B.G.W. was supported by a Boehringer Ingelheim Fonds PhD Fellowship. S.T. was supported by an Excellence Stipend of the Göttingen Graduate School for Neurosciences, Biophysics, and Molecular Biosciences (GGNB). The work was supported by grants to S.O.R. from the European Research Council (FP7 NANOMAP and ERC-2013-CoG NeuroMolAnatomy) and from the Deutsche Forschungsgemeinschaft (DFG) Cluster of Excellence Nanoscale Microscopy and Molecular Physiology of the Brain, as well as from DFG grants RI 1967 2/1, RI 1967 3/1, and SFB 889/A5. We acknowledge support by the DFG to V.H. (Exc-257-Neurocure and SFB 958/A01), H.U. (SFB 889), and M.K. (SFB 958/A11). Author contributions: B.G.W. prepared the synaptosomes and performed all immunoblotting experiments. K.K. performed the electron microscopy imaging and all neuromuscular junction imaging. C.S. performed the hippocampal culture imaging. S.T. performed the synaptosome imaging. B.R. generated the synapse model. S.J.K., G.A.C., and M.K. participated in the biochemistry experiments. S.M. and H.U. designed and performed all mass spectrometry experiments. S.O.R., B.G.W., and V.H. designed the experiments. All authors analyzed the data and contributed to writing the manuscript.

SUPPLEMENTARY MATERIALS

www.sciencemag.org/content/344/6187/1023/suppl/DC1
Materials and Methods
Figs. S1 to S7
Tables S1 to S3
Movie S1
References (*35*–*46*)

3 March 2014; accepted 6 May 2014
10.1126/science.1252884

CONSERVATION ECOLOGY

Optimal approaches for balancing invasive species eradication and endangered species management

Adam Lampert,[1]* Alan Hastings,[1] Edwin D. Grosholz,[1] Sunny L. Jardine,[2] James N. Sanchirico[1,3]

Resolving conflicting ecosystem management goals—such as maintaining fisheries while conserving marine species or harvesting timber while preserving habitat—is a widely recognized challenge. Even more challenging may be conflicts between two conservation goals that are typically considered complementary. Here, we model a case where eradication of an invasive plant, hybrid *Spartina*, threatens the recovery of an endangered bird that uses *Spartina* for nesting. Achieving both goals requires restoration of native *Spartina*. We show that the optimal management entails less intensive treatment over longer time scales to fit with the time scale of natural processes. In contrast, both eradication and restoration, when considered separately, would optimally proceed as fast as possible. Thus, managers should simultaneously consider multiple, potentially conflicting goals, which may require flexibility in the timing of expenditures.

Ecosystem-based management recognizes that managing individual species does not account for trade-offs and interactions with natural and human communities (*1*, *2*). Yet, the development of this approach has been limited by an absence of attempts to address conflicting goals and interactions. Conflicting goals may occur when two or more species or entities are being manipulated, such as when harvest of commercial fishes threatens endangered marine species via by-catch (*3*–*7*), when timber harvest destroys habitats of endangered wildlife species (*8*, *9*), and when supplying water at a high quantity reduces water quality at the source reservoir (*10*). Here, we focus on a particularly instructive example, where eradication of an invasive species (*11*–*13*) threatens the recovery of an endangered species (*14*–*16*). By modeling this case study, we suggest a general framework for managing conservation conflicts where actions for reaching one management goal have negative impacts on another goal. We begin with a description of the specific system and the conflicting management efforts directed at the two species.

Species of cordgrass in the genus *Spartina* have invaded many salt marshes around the world, which has resulted in changes to physical, biogeochemical, and biological processes that support benthic food webs and ecosystem productivity (*17*, *18*). *Spartina* invasions have also had an impact on human economies by altering shoreline geomorphology, affecting aquaculture, and reducing property values (*19*). Consequently, efforts to eradicate invasive *Spartina* have occurred worldwide (*19*). In San Francisco Bay, California, *S. alterniflora* was introduced from the eastern United States in the mid-1970s (*20*). It then hybridized with native *S. foliosa* and ultimately invaded ~800 acres (*21*) (Fig. 1A). Eradication of hybrid invasive *Spartina* began in 2005 and, to date, ~92% has been removed (Fig. 1B) (*22*). However, native *Spartina* has been slow to recover after eradication of the invader.

During the invasive *Spartina* eradication period, between 2005 and 2011, populations of the federally endangered California clapper rail (*Rallus longirostris obsoletus*) in San Francisco Bay declined by nearly 50% (*23*), presumably because of the overall decline in cover of *Spartina* in which clapper rail nests and forages. Thus, the U.S. Fish and Wildlife Service prohibited further eradication of invasive *Spartina* in the remaining untreated infested areas, which cover ~8% of the originally infested area. To allow completion of invasive *Spartina* eradication within the areas currently off limits without further losses of clapper rail habitat, restoration of native *Spartina* using nursery plants began in 2012.

To determine whether restoring native *Spartina* is cost-effective, and if so, how to best allocate efforts and a budget over time to combine native *Spartina* restoration with invasive *Spartina* eradication, we developed a theoretical model of *Spartina* management and estimated parameters for the model based on field data that was collected over several years (Fig. 2) (*24*). In addition to the distinction between native and invasive *Spartina*, we used a density-structured model (*25*) and further distinguished between two types of each *Spartina* species, "isolates" and "meadows." For invasive *Spartina*, isolates include individual plants that remain after treatment and new seedlings produced by remaining plants, whereas meadows are dense mature stands of untreated invasive *Spartina* that cover large areas. For native *Spartina*, isolates include naturally produced seedlings and restored individual plants, whereas meadows are dense mature stands covering larger areas. This distinction is important because clapper rails prefer larger meadows and are less willing to use individual plants as their habitat (*21*). Therefore, constraining the total amount of meadows (of either invasive or native *Spartina*) to remain above a certain limit is a plausible approach to promote the recovery of clapper rail while still allowing cost-effective management planning for the eradication program.

[1]University of California, Davis, One Shield Avenue, Davis, CA 95616, USA. [2]University of Delaware, Newark, DE 19716, USA. [3]Resources for the Future, Washington, DC 20036, USA.
*Corresponding author. E-mail: alampert@ucdavis.edu